ADAPTIVE FINITE ELEMENT METHOD TO DETERMINE K_I AND K_{II} OF CRACK PLATE WITH DIFFERENT $E_{INCLUSION}/E_{PLATE}$ RATIO

Wiroj Limtrakarn[1], Pramote Dechaumphai[2]
[1] *Department of Mechanical Engineering, Thammasat University, Rungsit Campus, Pathumthani, Thailand*
[2] *Department of Mechanical Engineering, Chulalongkorn University, Bangkok, Thailand*
E-mail: limwiroj@engr.tu.ac.th

Received July 2010, Accepted July 2011
No. 10-CSME-57, E.I.C. Accession 3220

ABSTRACT

An adaptive finite element method is presented to determine the K_I and K_{II} stress intensity factors of crack plate with different inclusions. The paper starts from describing two-dimensional fracture mechanics theory, an adaptive finite element formulation and the reflection photoelastic technique. An adaptive finite element method is evaluated by analyzing two examples. A single edge cracked plate made from polycarbonate. The second example is the slant edge 45° cracked plate subjected to a uniform uniaxial tensile stress. The K_I and K_{II} results are found to be function of the crack length per width and the inverse function of E ratio. These examples demonstrate the efficiency of the adaptive finite element method to provide accurate solutions as compared to those from the reflection photoelastic technique.

Keywords: adaptive finite element method; stress intensity factor; different E ratio.

DÉTERMINATION K_I ET K_{II} D'UNE PLAQUE FISSURÉE AVEC DIFFÉRENTS RATIOS $E_{INCLUSION}/E$ À L'AIDE DE LA MÉTHODE DES ÉLÉMENTS FINIS ADAPTÉS

RÉSUMÉ

La méthode des éléments finis adaptés est appliquée pour déterminer le K_I et K_{II} des facteurs d'intensité de contrainte d'une plaque fissurée avec différentes inclusions. L'article commence par expliquer la théorie de la mécanique de la fissure bi-dimensionnelle, ainsi que la formulation des éléments finis adaptés et la technique de la réflexion photoélastique. Une méthode des éléments finis adaptés est évaluée par l'étude de deux exemples. Le premier exemple est une plaque fissurée à bord simple fabriquée en polycarbonate. Le deuxième est une plaque fissurée avec un bord en 45°degré soumis à une contrainte d'intensité uniforme uniaxiale. Les résultats K_I et K_{II} sont en fonction de la largeur de la fissure et la fonction inverse de ratio E. Ces exemples démontrent l'efficacité de la méthode des éléments finis adaptés pour apporter des solutions adéquates de comparaison avec la technique de réflexion photoélastique.

Mots-clés : méthodes des éléments finis adaptés; facteurs d'intensité de contrainte; *E*ratio différent.

1 INTRODUCTION

Light weight composite materials ($E_{inclusion}/E_{plate}$ ratio $\neq 1$) are important and widely used in many applications recently. Appropriate mechanical properties of the matrix and inclusions in these composite materials affect their product life. The life prediction of composite products is one of the most important studies in engineering design and maintenance. Crack propagation is one of the key behaviors to assess the life of the composite products. The stress intensity factors determination near crack tip on composite material are needed to predict the crack propagation accurately. Several numerical methods and nondestructive experimental techniques are currently used to determine such phenomena. The reflection photoelastic technique with an optic–experimental interference has been employed to determine the stress intensity factors and inclusion effect [1–5]. Its principle is based on the double refraction phenomenon by analyzing the maximum shear stress induced in the transparent or birefringent of the photoelastic model under loading. The phenomenon is observed by looking through the optical elements, i.e., the polarizer and analyzer of the polariscope as shown in Fig. 1. Their results provide information that can be applied directly to metal prototypes by using the law of similarity. At present, several numerical methods have also been developed to predict stress intensity factor. These methods include the finite element method [6–8], the meshless method [9–10], the manifold method with virtual crack extension [11], and the boundary element method [12–13].

In this paper, the stress intensity factors K_I and K_{II} of the crack plate with different $E_{inclusion}/E_{plate}$ ratio are determined by using the adaptive finite element method. Theory of two-dimensional fracture mechanics is first described. The finite element method using the 8-node quadrilateral elements surrounding the crack tip together with the adaptive meshing technique are explained. The finite element formulation and its computational procedure are described. The adaptive meshing technique is explained. The reflection photoelastic technique is then presented for determining the stress intensity factors. The adaptive finite element method is evaluated by benchmark problems. The first problem is the single edge cracked plate under tensile loading. Their results obtained from the adaptive finite element method are compared with the reflection photoelastic technique and those presented by Brown [14]. Three additional cracked plate configurations, i.e. plate with a hole, without and with soft and hard inclusions, are investigated. The second problem is the slant edge cracked plates with 45° crack edge inclination subjected to a uniform tensile loading. The adaptive finite element solution of neat polycarbonate is compared with the reflection photoelastic technique solution and the empirical formula of Freeze [15] for different crack length ratios. Three additional configurations of plate similar to the first example are also investigated. Solutions obtained from the adaptive finite element method solution are compared with those of the reflection photoelastic technique.

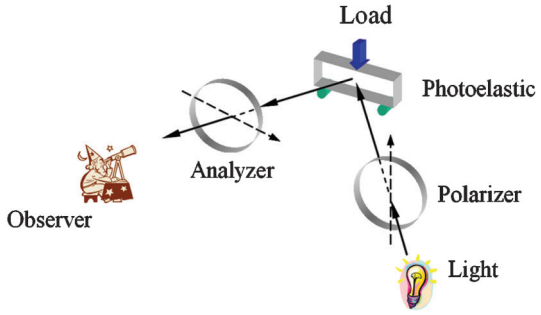

Fig. 1. Photoelastic model under loading in reflection polariscope.

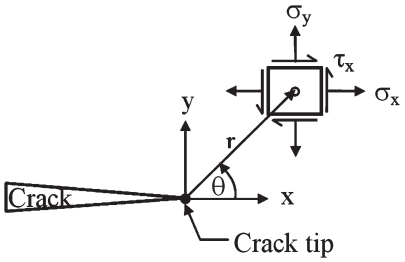

Fig. 2. State of stresses in polar coordinates from crack tip.

2 THEORY

2.1 Stress and Stress Intensity Factor Relations

The relations of the stress and stress intensity factors for mode *I* and *II* using the Linear Elastic Fracture Mechanics (LEFM) theory are [16],

$$\sigma_x = \frac{1}{\sqrt{2\pi r}}\left[K_I \cos\frac{\theta}{2}\left(1-\sin\frac{\theta}{2}\sin\frac{3\theta}{2}\right) - K_{II}\sin\frac{\theta}{2}\left(2+\cos\frac{\theta}{2}\cos\frac{3\theta}{2}\right)\right] \tag{1}$$

$$\sigma_y = \frac{1}{\sqrt{2\pi r}}\left[K_I \cos\frac{\theta}{2}\left(1-\sin\frac{\theta}{2}\sin\frac{3\theta}{2}\right) - K_{II}\sin\frac{\theta}{2}+\cos\frac{\theta}{2}\cos\frac{3\theta}{2}\right] \tag{2}$$

$$\tau_{xy} = \frac{1}{\sqrt{2\pi r}}\left[K_I \sin\frac{\theta}{2}\cos\frac{\theta}{2}\cos\frac{3\theta}{2} + K_{II}\cos\frac{\theta}{2}\left(1-\sin\frac{\theta}{2}\sin\frac{3\theta}{2}\right)\right] \tag{3}$$

where K_I and K_{II} are the stress intensity factors for the opening mode (mode *I*) and the tearing mode (mode *II*); r and θ are the distance and the angle in the polar coordinates as shown in Fig. 2; σ_x and σ_y are the normal stresses in x and y directions, respectively, and τ_{xy} is the shearing stress.

The general form of the stress intensity factor at the crack tip is given by [17],

$$K = F\sigma_\infty\sqrt{\pi a} \tag{4}$$

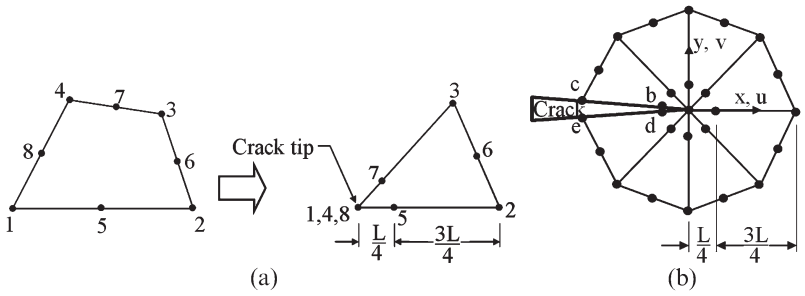

Fig. 3. Eight-node quadrilateral element around crack tip. (a) A quarter–point eight–node quadrilateral element. (b) Quarter–point quadrilateral elements around crack tip.

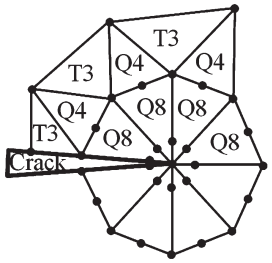

Fig. 4. Combination of three element types surrounding crack tip.

where F is the geometry factor that depends on the dimensions of problem, σ_∞ is the far–field stress and a is the crack length.

The stress intensity factors K_I and K_{II} can be determined from displacement extrapolation near the crack tip. These stress intensity factors are expressed by,

$$K_I = \frac{E}{3(1+v)(1+\kappa)}\sqrt{\frac{2\pi}{L}}\left(4(v_b - v_d) - \left(\frac{v_c - v_e}{2}\right)\right) \tag{5}$$

$$K_{II} = \frac{E}{3(1+v)(1+\kappa)}\sqrt{\frac{2\pi}{L}}\left(4(u_b - u_d) - \left(\frac{u_c - u_e}{2}\right)\right) \tag{6}$$

Where E is the modulus of elasticity, v is the Poisson's ratio, κ is the elastic parameter defined by $(3-4v)$ for plane strain case and $(3-v)/(1+v)$ for plane stress case, L is the element length, u and v are the displacement components in $x-$ and $y-$directions, respectively. The subscripts of u and v represent their positions for the nodes of the elements surrounding the crack tip as shown in Fig. 3(a). Figure 3(b) provides detail of the eight-node quadrilateral element with their mid-side node positions, while nodes 1, 4 and 8 are collapsed and placed together at the crack tip.

2.2 Finite Element Method

The finite element equations can be derived from the governing differential equations of equilibriums. The derived finite element equations are written in matrix form as,

$$[K]\{\delta\} = \{F\} \tag{7}$$

where $\{\delta\}$ is the vector of the element nodal displacements, $[K]$ is the element stiffness matrix [18] and $\{F\}$ is the element load vector.

To obtain a solution with good accuracy around the crack tip, the finite elements with high-order element interpolation functions are preferred. The eight–node quadrilateral elements (Q8) are selected herein to construct a circular zone surrounding the crack tip. These elements have their mid–side nodes displaced from their nominal position to quarter points of the tip as shown in Fig. 3(a). The radius of the circular zone is specified to be no longer than one–eight of the initial crack length, with roughly one element every 30° in the circumferential direction [19].

The four–node quadrilateral elements (Q4) are also chosen to connect the Q8 elements at the crack tip with the triangular elements (T3) in the regions away from the crack tip as shown in Fig. 4.

2.3 Adaptive Meshing Technique

Adaptive mesh generation techniques may be classified into two major categories: 1) refinement/derefinement, and 2) remeshing. The first category, the adaptive refinement/redefinement technique, can be further classified into three subcategories: a) the *h* method, b) the *p* method, and c) the *r* method. In the *h* method, the elements in the initial mesh are refined into smaller elements or derefined into larger elements [20]. The *p* method maintains the geometry of the elements of the initial mesh but increases (or decreases) the order of the polynomials used for the element interpolation functions [21]. The *r* method keeps the number of elements and their connectivities the same but relocates the nodes [22].

The remeshing technique, the second adaptive mesh-generation category, generates an entirely new mesh based on the solution obtained from an earlier mesh [23, 24]. The idea is to construct a new mesh that consists of small elements in the regions with large change in solution gradients and large elements in the other regions where the changes in solution gradients are small. To determine appropriate element sizes at different locations in the domain, the von Mises stress σ is used as the indicator for computing proper element sizes. As small elements are required in the region where changes in the von Mises stress gradients are large, the second derivatives of the von Mises stress at a point with respect to global coordinates x and y are needed. By using the concept of principal directions from a given state of stresses at a point, the principal quantities in the principal directions X and Y where the cross-derivatives vanish are determined:

$$\begin{bmatrix} \dfrac{\partial^2\sigma}{\partial x^2} & \dfrac{\partial^2\sigma}{\partial x\partial y} \\ \dfrac{\partial^2\sigma}{\partial x\partial y} & \dfrac{\partial^2\sigma}{\partial y^2} \end{bmatrix} \Rightarrow \begin{bmatrix} \dfrac{\partial^2\sigma}{\partial X^2} & 0 \\ 0 & \dfrac{\partial^2\sigma}{\partial Y^2} \end{bmatrix} \tag{8}$$

The principal quantities of each element are then determined,

$$\lambda_1 = \left|\frac{\partial^2\sigma}{\partial X^2}\right| \text{and } \lambda_2 = \left|\frac{\partial^2\sigma}{\partial Y^2}\right| \tag{9}$$

These principal quantities are then used to compute proper element sizes h_1 and h_2 in the two principal directions using the condition [25],

$$h_1^2\lambda_1 = h_2^2\lambda_2 = \text{constant} = h_{\min}^2\lambda_{\max} \tag{10}$$

where $h_{\min}$ is the specified minimum element size, and $\lambda_{\max}$ is the maximum principal quantity for the entire model.

Based on the condition shown in Eq. (10), the element size is generated according to the given minimum element size $h_{\min}$ Specifying too small $h_{\min}$ may result in a model with an excessive number of elements. On the other hand, specifying too large $h_{\min}$ may result in an inadequate solution accuracy or excessive analysis and meshing cycles. These factors must be considered prior to generating a new mesh. Note that, because the technique generates an entirely new mesh with different nodal locations from the old mesh, interpolation of the solution from the old to the new mesh should be used to increase the analysis solution convergence.

2.4 Reflection Photoelasticity Technique

The reflection photoelastic technique can be used to determine the state of stresses and crack speed on a transparent material under both the static and dynamic conditions [26]. The technique provides relationships of the direct isochromatic-fringe-pattern and the difference of the principle stresses as,

$$\sigma_1 - \sigma_2 = 2\tau_m = \frac{Nf_\sigma}{2t} \tag{11}$$

where τ_m is the maximum in–plane shear stress, f_σ is the stress–optical constant, N is the order of the isochromatic fringe, and t is the specimen thickness.

The maximum shear stress is related with the stress components in the form,

$$(2\tau_m)^2 = (\sigma_x - \sigma_y)^2 + 4\tau_{xy}^2 \tag{12}$$

Similarly, by substituting Eq. (1) – (3) into Eq. (12), the relationship between the maximum shear stress and the stress intensity factors is obtained [27],

$$\begin{aligned}(2\tau_m)^2 = {} & \frac{1}{2\pi r}\left[(K_I \sin\theta + 2K_{II}\cos\theta)^2 + (K_{II}\sin\theta)^2\right] + \\ & \frac{2}{\sqrt{2\pi r}}\sin\frac{\theta}{2}\left[K_I \sin\theta(1+2\cos\theta)\right] + K_{II}\left(1+2\cos^2\theta+\cos\theta\right)\end{aligned} \tag{13}$$

Similarly, by substituting Eq. (11) into Eq. (13), the stress intensity factor for the opening mode can be expressed in the form,

$$K_I = \frac{Nf_\sigma}{2t}\frac{\sqrt{2\pi r_m}}{\sin\theta_m}\left[1+\left(\frac{2}{3\tan\theta_m}\right)^2\right]^{-\frac{1}{2}}\left(1+\frac{2\tan\frac{3\theta_m}{2}}{3\tan\theta_m}\right) \tag{14}$$

where θ_m is the angle of inclination to the crack plane, r_m is the distance from crack tip to the farthest point on a given isochromatic loop as shown in Fig. 5. The position of the farthest point on a given isochromatic loop is represented by $\frac{\partial \tau_m}{\partial \theta} = 0$.

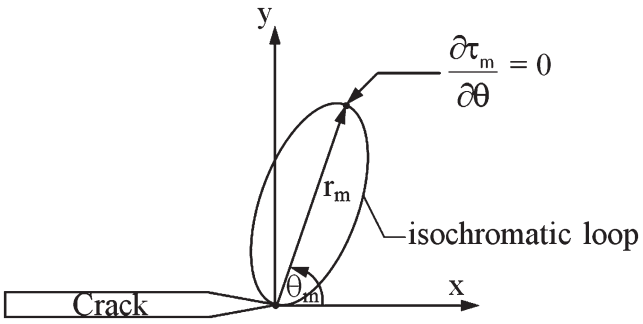

Fig. 5. Distance rm and angle θm of isochromatic loop.

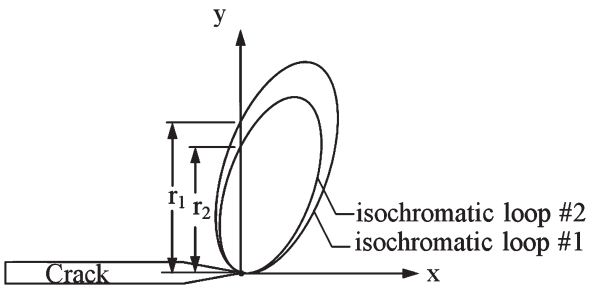

Fig. 6. Distance r_m of two isochromatic loop.

The relationship between the stress intensity factors and the angle θ_m is obtained by minimizing Eq. (13) with respect to θ to yield,

$$\left(\frac{K_{II}}{K_I}\right)^2 - \frac{4}{3}\left(\frac{K_{II}}{K_I}\right)\cot 2\theta_m - \frac{1}{3} = 0 \tag{15}$$

Equation (15) above is used to determine the ratio (K_{II}/K_I) by measuring the angle θ_m on the isochromatic loop which is valid at the point very closed to the crack tip. By using the measured data from the two isochromatic loops along the line perpendicular to the crack plane ($\theta = 90^\circ$) [28] as shown in Fig. 6, the stress intensity factor can be computed from [27],

$$K_I = \frac{f_\sigma}{2t}\sqrt{2\pi r_1}\,\frac{(N_1 - N_2)}{1 - \sqrt{(r_1/r_2)}} \tag{16}$$

3 APPLICATIONS

The adaptive finite element method is evaluated by using the two benchmark problems of a single edge cracked plate and a slant edge cracked plate with 45° crack edge, all under uniaxial tensile loading. The plates have dimensions of $36 \times 72 \times 3mm$ and are made from polycarbonate material ($PS1$) for which a side is coated by resin & diethylenetriamine with silver color. Isopropyl alcohol is required to degrease and clean the coating surfaces. A neat plate, plate with

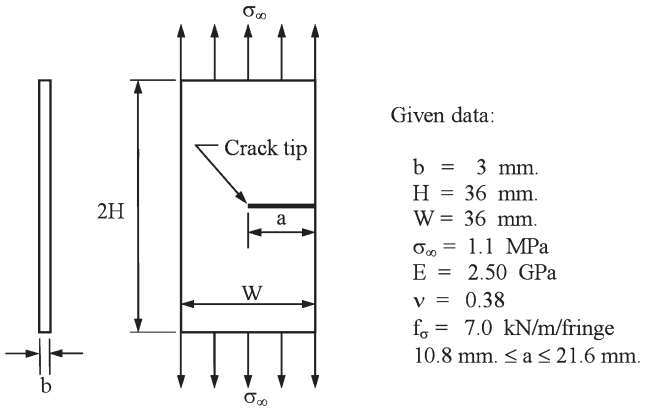

Fig. 7. Problem statement of single edge cracked plate under tensile loading.

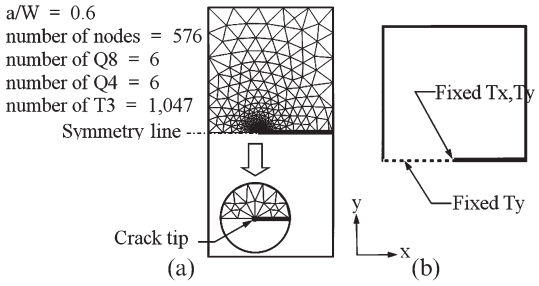

Fig. 8. Adaptive finite element model of single edge cracked plate with $a/W = 0.6$. (a) Adaptive finite element model. (b) Boundary conditions.

a hole, plates with a hole plus soft and hard inclusions are studied. The soft inclusion is made of Teflon with the E_{soft}/E_{PS1} ratio $= 0.24$ while the hard inclusion is made of magnesium alloy AZ61 with E_{hard}/E_{PS1} ratio $= 18$.

3.1 Single Edge Crack Edge Tension

A rectangular plate, with varied crack length per width (a/W) between 0.3 to 0.60.6, is used in the study. The plate is subjected to a far–field tensile stress of $\sigma_\infty = 1.1 MPa$ along the top and bottom edges as shown in Fig. 7. Due to symmetry of the problem, only the upper half of the plate is used as a finite element model. Four analysis cases were performed with the crack length per width of 0.3, 0.4, 0.5 and 0.6. As an example for the case of the crack length per width of 0.6, the adaptive finite element mesh containing six Q8-elements, six Q4-elements and 1,047 of the T3 elements, with the total of 576 nodes is shown in Fig. 8.

It is noted that the stress intensity factor given by Brown [14] for this problem is,

$$K_I = \sigma_\infty \sqrt{\pi a}\left[1.122 - 0.231\frac{a}{W} + 10.55\left(\frac{a}{W}\right)^2 - 21.71\left(\frac{a}{W}\right)^3 + 30.382\left(\frac{a}{W}\right)^4\right] \tag{17}$$

The computed stress intensity factor for the opening mode K_I obtained from the adaptive finite element method and the reflection photoelastic technique is 1.22410 and 1.22271, as compared to 1.22074 from Eq. (17) with the differences of 0.28% and 0.16%, respectively.

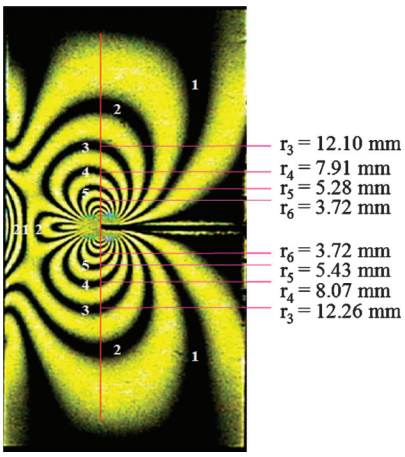

Fig. 9. Photoelastic result of single edge cracked plate with $a/W = 0.6$.

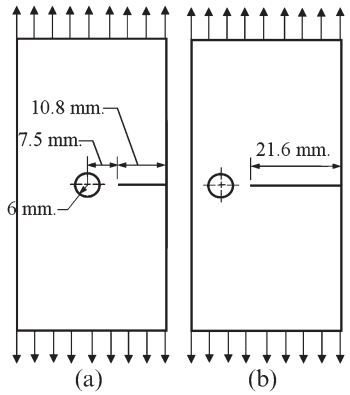

Fig. 10. Position of a hole varied with crack length ratios on single edge cracked plate. (a) $a/W=0.3$. b) $a/W=0.6$.

Figure 9 shows the reflection photoelastic result using the photo camera technique [22] for the neat plate of $a/W=0.6$. The measured values of r_1 for each N_i, $i=1$ to 4, for the top and bottom fringe images are used to calculate the average stress intensity factors. Figure 10 shows the position of the hole that varies with the crack length ratios. In this example four analysis cases of crack length ratios of 0.3, 0.4, 0.5 and 0.6 as well as the three cases of a plate with a hole, a plate with hole plus soft and hard inclusions, are investigated.

The stress intensity factor K_I results of the neat plate obtained from the finite element method and the reflection photoelasticity technique are compared with those given by Brown for $a/W=0.3$, 0.4, 0.5 and 0.6 as shown in Fig. 11. The figure shows good agreement of the solutions for all cases of the crack length ratio. In these cases, the average K_I difference of adaptive finite element method and reflection photoelasticity technique is by about 5.57%. Figure 11 also shows the stress intensity factor K_I obtained from both methods for the plates with a hole plus soft and hard inclusions. For all cases of the crack length ratio, the stress intensity factor K_I for the hard inclusion is highest while that of the neat plate is smallest. The average stress intensity factor K_I for the neat plate is greater by about 3.07% (E ratio $=18$) than that of the plate with hard inclusion. It is also greater than that of the plate with soft inclusion

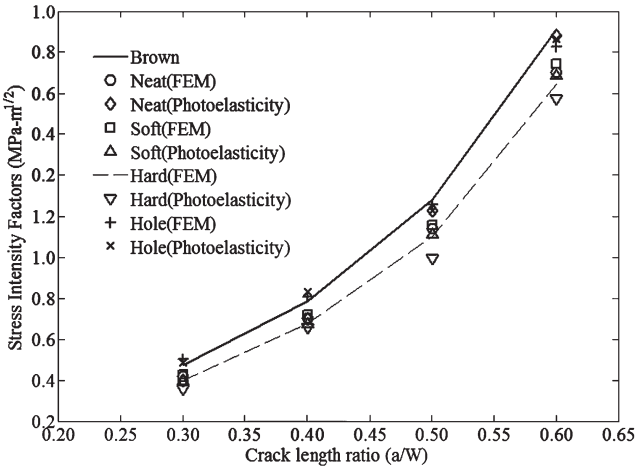

Fig. 11. Comparative stress intensity factor K_I for single edge cracked plate.

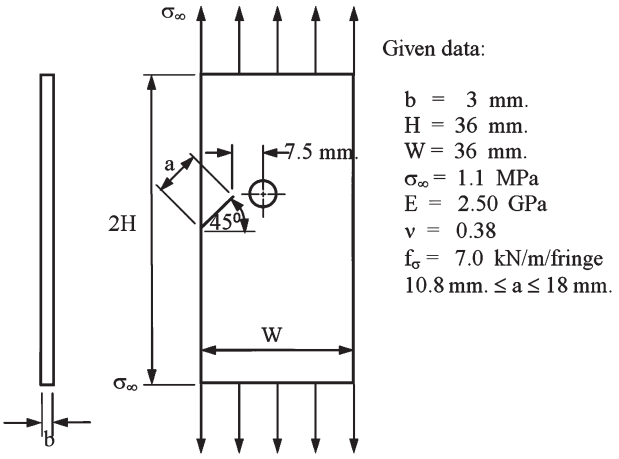

Fig. 12. Problem statement of slant edge cracked plate under tensile loading.

and the plate without inclusion by about 1.55% (E ratio $=0.24$) and 9.86% (E ratio $=0$), respectively.

3.2 Slant Edge Crack Edge Tension with 45° Crack Edge

The geometry and material properties of the plate in this example are the same as those in the previous one. The crack has 45° inclined angle with the horizontal line as shown in Fig. 12. Under the tensile loading, σ_∞, an inclined crack with mixed mode occurs. Figure 13 shows an adaptive finite element mesh with 4,890 nodes, 8 Q8-elements, 8 Q4-elements and 9,430 of the T3-elements as well as boundary conditions.

The photoelastic fringe image for the case of $a/W=0.3$ is shown in Fig. 14. The stress intensity factor K_I is computed by measuring the distance r_m of the isochromatic fringe loop number 2 and 3, and substituting them into Eq. (16). The stress intensity factor K_{II} is determined by measuring the angle θ_m on the isochromatic loop and substituting it into Eq. (12). Figure 15 shows the position of the hole with the varied crack length ratios of 0.3, 0.4 and 0.5. In this example, the plates with a hole without and with soft and hard inclusions are studied. The stress intensity factors K_I, K_{II} are determined in the same fashion as explained earlier.

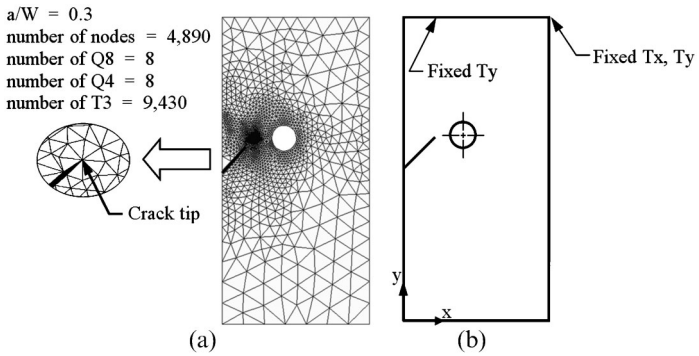

Fig. 13. Adaptive finite element model of slant edge cracked plate with $a/W=0.3$. (a) Adaptive finite element model. (b) Boundary condition.

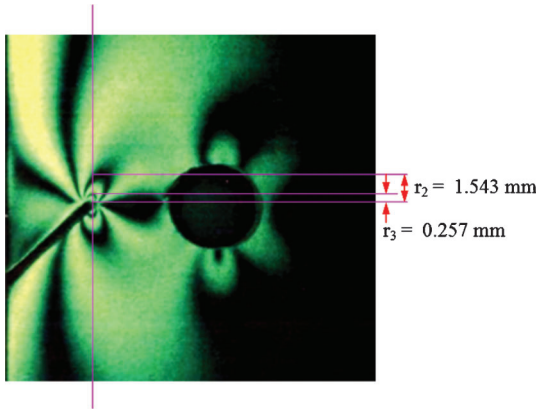

Fig. 14. Photoelastic result of slant edge cracked plate with $a/W = 0.3$.

The stress intensity factor K_I, K_{II} results from the adaptive finite element method and the reflection photoelasticity technique for the plate without and with the soft and hard inclusions, together with the three crack length ratios, $a/W = 0.3$, 0.4, and 0.5, are compared with those given by Freeze [15] as shown in Fig. 16 and 17. In all cases, the average K_I and K_{II} differences of adaptive finite element method and reflection photoelasticity technique are by about 3.23% and 4.23%, respectively. The figures show good agreement of the solutions for all cases of the crack length ratio. In these cases, the stress intensity factors K_I and K_{II} with the hard inclusion are smallest while those of plate without inclusion are highest. The average stress intensity factors K_I and K_{II} of neat plate are higher than those of the plate with hard inclusion (E ratio $=18$) by about 6.82% and 9.81%, respectively. These stress intensity factors are smaller than those of the plate with soft inclusion (E ratio $=0.24$) by about 0.91% and 0.06%, respectively, and the plate without inclusion (E ratio $=0$) by about 11.07% and 19.23%, respectively.

4.CONCLUSIONS

An adaptive finite element method using the eight-node quadrilateral finite element surrounding the crack tip is presented to analyze two-dimensional fracture mechanics problems. The method is used to determine the stress intensity factors for plates with cracks. The adaptive finite element method generates small elements in the crack region to capture high stress gradients to provide high solution accuracy. Larger elements are generated in the other

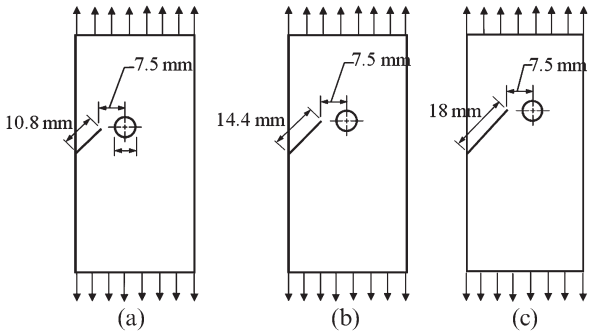

Fig. 15. Position of a hole varied with crack length ratios on slant edge cracked plate. (a) $a/W = 0.3$. (b) $a/W = 0.4$. (c) $a/W = 0.5$.

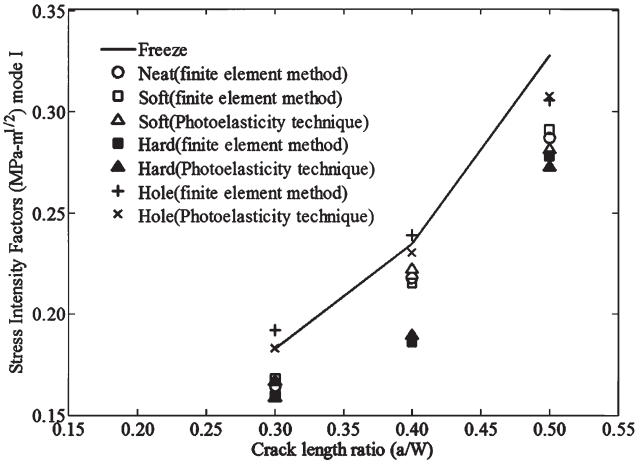

Fig. 16. Comparative stress intensity factor K_I for slant edge cracked plate.

regions where the stress gradients are small to reduce number of elements and thus the computational time. The reflection photoelastic technique is also employed to obtain the stress intensity factors. The benchmarks problems of: (1) single edge cracked plate and (2) slant edge cracked plate, under tensile loading were used to evaluate the performance of the adaptive finite element method. The plates with a hole along with soft and hard inclusions are used in the study. Results of the stress intensity factors obtained from the adaptive finite element method and reflection photoelastic technique are compared. The accuracy of photoelasticity results depends on the fringe image resolution of the camera and the number of fringes around the crack tip. In the example of the single edge cracked plate, the stress intensity factor K_I of the plate with hard inclusion is smallest while that of plate without inclusion is highest. The stress intensity factor K_I of the plate with soft inclusion is greater than that of the plate with hard inclusion and the neat plate, but is less than that of plate without inclusion. In the example of the slant edge cracked plate, the stress intensity factors K_I and K_{II} obtained from the adaptive finite element method and the reflection photoelastic technique agree very well. The stress intensity factors K_I and K_{II} of the plate with hard inclusion are lowest while those for the plate

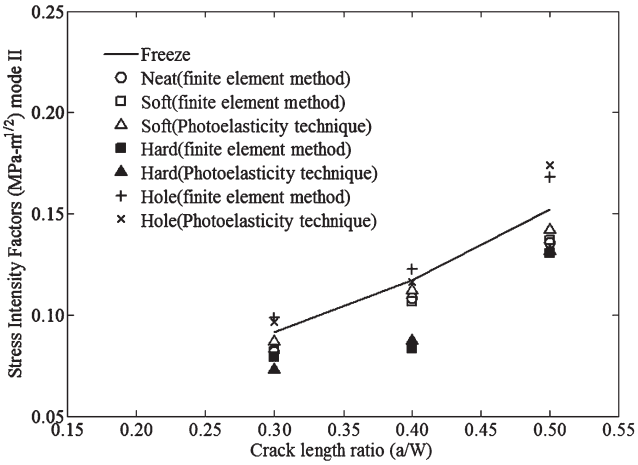

Fig. 17. Comparative stress intensity factor K_{II} for slant edge cracked plate.

without inclusion are highest. The stress intensity factors K_I and K_{II} of the plate with soft inclusion are less than those for the plate with hard inclusion and the neat plate, but greater than those for the plate without inclusion. These examples have demonstrated the applicability and advantages of the adaptive finite element method for providing accurate prediction of the stress intensity factors.

ACKNOWLEDGEMENTS

The authors are pleased to acknowledge the Thailand Commission on Higher Education of Thailand (the National Research University Project), Thammasat University, the Thailand Research Fund (TRF), and the National Research Council of Thailand (NRCT) for supporting this research work.

REFERENCES

1. Jenkins, D.R., ''Analysis of behavior near a cylindrical glass inclusion by scattered-light photoelasticity,'' *Experimental Mechanics*, Vol. 8, No. 10, pp. 467–473, 1968.
2. Toole, B.J.O. and Santare, M.H., ''Photoelastic investigation of crack-inclusion interaction,'' *Experimental Mechanics*, Vol. 30, No. 3, pp. 253–257, 1990.
3. Sushschenko, S.A., ''Photoelastic Analysis of Stress Concentrations in a Two-Dimensional Model of Hard Inclusions in a Metal Matrix,'' *Tribology Transactions*, Vol. 40, No. 2, pp. 386–390, 1997.
4. Nugent, E.E., Calhoun, R.B. and Mortensen, A., ''Experimental Investigation of Stress and Strain Fields in a Ductile Matrix Surrounding an Elastic Inclusion,'' *Acta Materialia*, Vol. 48, No. 7, pp. 1451–1467, 2000.
5. Corso, F.D., Bigoni, D. and Gei, M., ''The Stress Concentration near a Rigid Line Inclusion in a Prestressed,'' *Journal of the Mechanics and Physics of Solids*, Vol. 56, No, 3, pp. 815–838, 2008.
6. Kim, J.H. and Paulino, G.H., ''Simulation of crack propagation in functionally graded materials under mixed–mode and non–proportional loading,'' *International Journal of Mechanics and Materials in Design*, Vol. 1, No. 1, pp. 63–94, 2004.
7. Phongthanapanich, S. and Dechaumphai, P., ''Adaptive Delaunay triangulation with object–oriented programming for crack propagation analysis,'' *Finite Element in Analysis and Design*, Vol. 40, No. 13–14, pp. 1753–1771, 2004.
8. Alshoaibi, A.M., Hadi, M.S.A. and Ariffin, A.K., ''An adaptive finite element procedure for crack propagation analysis,'' *Journal of Zheijang Univeristy Science A*, Vol. 8, No. 2, pp. 228–236, 2006.
9. Rao, B.N. and Rahman, S., ''An efficient meshless method for fracture analysis for cracks,'' *Computational Mechanics*, Vol. 26, No. 4, pp. 398–408, 2000.
10. Luliang, L. and Pan, Z., ''Meshless method for 2D mixed–mode crack propagation based on voronoi cell,'' *Acta Mechanica Solida Sinica*, Vol. 16, No. 3, pp. 231–239, 2003.
11. Chiuo, Y.J., Lee, Y.M. and Tsay, R.J., ''Mixed mode fracture propagation by manifold method,'' *International Journal of Fracture*, Vol. 114, No. 4, pp. 327–347, 2002.
12. Xu, K., Lie, S.T. and Cen, Z., ''Crack propagation analysis with Galerkin boundary element method,'' *International Journal for Numerical and Analytical Methods in Geomechanics*, Vol. 22, No. 5, pp. 421–435, 2004.
13. Kitey, R., Phan, A.V., Tippur, H.V. and Kaplan, T., ''Modeling of Crack Growth Through Particulate Clusters in Brittle Matrix by Symmetric–Galerkin Blundary Element Method,'' *International Journal of Fracture*, Vol. 141, No. 1–2, pp. 11–25, 2006.

14. Hiroshi, T., Paul, C.P. and George, R.I., *The Stress Analysis of Crack Handbook*, ASME, 1985.
15. Murakami, Y., *Stress Intensity Factors Handbook*, Pergamon Press, Vol. 2, pp. 916–918, 1986.
16. Anderson, T.L, *Fracture Mechanics: Fundamentals and Applications*, CRC Press, 1994.
17. Limtrakarn, W., "Stress Analysis on Crack Tip Using Q8 and Adaptive Meshes," *Thammasat International Journal of Science and Technology*, Vol. 10, No. 1, pp. 19–24, 2005.
18. Zienkiewicz, O.C and Taylor, R.L, *Finite element method*, 5th Edition, Woburn, Butterworth–Heinemann, 2000.
19. Guinea, G.V, Planas, J. and Elices, M., "K evaluation by the displacement extrapolation technique," *Eng. Fract. Mech*. Vol. 66, No. 3, pp. 243–255, 2000.
20. Ramakrishnan, R., Bey, K. S. and Thornton, E. A. "Adaptive Quadrilateral and Triangular Finite-Element Scheme for Compressible Flows," *American Institute of Aeronautics and Astronautics -Journal*, Vol. 28, No.1, pp. 51–59, 1990.
21. Dechaumphai, P. "Improved Finite Element Methodology for Integrated Thermal-Structure Analysis," NASA CR 3635, 1982.
22. Lohner, R., Morgan, K. and Zienkiewicz, O. C. "Adaptive Grid Refinement for Compressible Euler and Navier-Stokes Equations," *The International Conference on Accuracy Estimates and Adaptive Refinements in Finite Element Computations*, New York, Wiley, Vol. 2, pp. 189–202, 1984.
23. Dechaumphai, P., "Adaptive Finite Element Technique for Heat Transfer Problems," *Journal of Energy, Heat & Mass Transfer*, Vol. 17, No. 2, pp. 87–94, 1995.
24. Peraire, J., Vahjdati, M., Morgan, K. and Zienkiewicz, O.C., "Adaptive Remeshing for Compressible Flow Computation," *Journal of Computational Physics*, Vol. 72, pp. 449–466, 1987.
25. Oden, J. T. and Carey, G. F. "Finite Elements: Mathematical Aspects" New Jersey, Prentice-Hall, 1981.
26. Irwin, G.R., "Discussion of The Dynamic Stress Distribution Surrounding a Running Crack – A Photoelastic Analysis," *Proc. Soc. Exp. Stress Analysis*, Vol. 16, No. 1, pp. 93–96, 1958.
27. Paipetis, S.A. and Holister, G.S., "Photoelasticity in Engineering Practice," *Elsevier Applied Science Publishers*, pp. 181–204, 1985.
28. Schroedl, M.A. and Smith, C.W., "Local Stress near Deep Surface Flaws under Cylindrical Bending Fields," *American Society for Testing and Materials special technical publication 536*, pp. 45–63, 1973.